Light trapping in ultrathin plasmonic solar cells

Vivian E. Ferry,[1,2,*] Marc A. Verschuuren,[3] Hongbo B. T. Li,[4] Ewold Verhagen,[1] Robert J. Walters,[1] Ruud E. I. Schropp,[4] Harry A. Atwater,[2] and Albert Polman[1]

[1]*Center for Nanophotonics, FOM Institute AMOLF, Science Park 104, 1098 XG Amsterdam, The Netherlands*
[2]*Thomas J. Watson Laboratories of Applied Physics, California Institute of Technology, Pasadena, California 91125 USA*
[3]*Philips Research Laboratories, High Tech Campus 4, 5656 AE Eindhoven, The Netherlands*
[4]*Debye Institute for Nanomaterials Science, Section Nanophotonics, Utrecht University, P. O. Box 80.000, 3508 TA Utrecht, The Netherlands*
**vianf@caltech.edu*

Abstract: We report on the design, fabrication, and measurement of ultrathin film a-Si:H solar cells with nanostructured plasmonic back contacts, which demonstrate enhanced short circuit current densities compared to cells having flat or randomly textured back contacts. The primary photocurrent enhancement occurs in the spectral range from 550 nm to 800 nm. We use angle-resolved photocurrent spectroscopy to confirm that the enhanced absorption is due to coupling to guided modes supported by the cell. Full-field electromagnetic simulation of the absorption in the active a-Si:H layer agrees well with the experimental results. Furthermore, the nanopatterns were fabricated via an inexpensive, scalable, and precise nanopatterning method. These results should guide design of optimized, non-random nanostructured back reflectors for thin film solar cells.

OCIS codes: (250.5403) Plasmonics; (350.6050) Solar Energy.

References and links

1. A. Shah, P. Torres, R. Tscharner, N. Wyrsch, and H. Keppner, "Photovoltaic technology: the case for thin-film solar cells," Science **285**(5428), 692–698 (1999).
2. R. H. Franken, R. L. Stolk, H. Li, C. H. M. van der Werf, J. K. Rath, and R. E. I. Schropp, "Understanding light trapping by light scattering textured back electrodes in thin film n-i-p-type silicon solar cells," J. Appl. Phys. **102**(1), 014503 (2007).
3. J. Müller, B. Rech, J. Springer, and M. Vanecek, "TCO and light trapping in silicon thin film solar cells," Sol. Energy **77**(6), 917–930 (2004).
4. R. E. I. Schropp, and M. Zeman, *Amorphous and microcrystalline silicon solar cells: modeling, materials, and device technology*, (Kluwer Academic Publishers, Norwell, Mass., 1998).
5. P. Campbell, and M. A. Green, "The limiting efficiency of silicon solar-cells under concentrated sunlight," IEEE Trans. Electron. Dev. **33**(2), 234–239 (1986).
6. D. L. Staebler, and C. R. Wronski, "Reversible conductivity changes in discharge-produced amorphous silicon," Appl. Phys. Lett. **31**(4), 292–294 (1977).
7. A. V. Shah, H. Schade, M. Vanecek, J. Meier, E. Vallat-Sauvain, N. Wyrsch, U. Kroll, C. Droz, and J. Bailat, "Thin-film Silicon Solar Cell Technology," Prog. Photovolt. Res. Appl. **12**(23), 113–142 (2004).
8. P. Lechner, W. Frammelsberger, W. Psyk, R. Geyer, H. Maurus, D. Lundszien, H. Watner, and B. Eichhorn, "Status of performance of thin film silicon solar cells and modules," Conference record of the 23rd European Photovoltaic Solar Energy Conference, 2023–2026 (2008).
9. E. Yablonovitch, and G. D. Cody, "Intensity enhancement in textured optical sheets for solar cells," IEEE Trans. Electron. Dev. **29**(2), 300–305 (1982).
10. Ü. Dagkaldiran, A. Gordijn, F. Finger, H. M. Yates, P. Evans, D. W. Sheel, Z. Remes, and M. Vanecek, "Amorphous silicon solar cells made with SnO2:F TCO films deposited by atmospheric pressure CVD," Mater. Sci. Eng. B **159–160**, 6–9 (2009).
11. J. Krč, F. Smole, and M. Topič, "Potential of light trapping in microcrystalline silicon solar cells with textured substrates," Prog. Photovolt. Res. Appl. **11**(7), 429–436 (2003).
12. S. Fahr, C. Rockstuhl, and F. Lederer, "Engineering the randomness for enhanced absorption in solar cells," Appl. Phys. Lett. **92**(17), 171114 (2008).
13. H. A. Atwater, and A. Polman, "Plasmonics for improved photovoltaic devices," Nat. Mater. **9**(3), 205–213 (2010).
14. V. E. Ferry, J. N. Munday, and H. A. Atwater, "Design considerations for plasmonic photovoltaics," Adv. Mater. (to be published).

#128370 - $15.00 USD Received 12 May 2010; revised 7 Jun 2010; accepted 8 Jun 2010; published 24 Jun 2010

15. H. R. Stuart, and D. G. Hall, "Island size effects in nanoparticle-enhanced photodetectors," Appl. Phys. Lett. **73**(26), 3815–3817 (1998).
16. S. Pillai, K. R. Catchpole, T. Trupke, and M. A. Green, "Surface plasmon enhanced silicon solar cells," J. Appl. Phys. **101**(9), 093105 (2007).
17. K. R. Catchpole, and A. Polman, "Design principles for particle plasmon enhanced solar cells," Appl. Phys. Lett. **93**(19), 191113 (2008).
18. F. J. Beck, A. Polman, and K. R. Catchpole, "Tunable light trapping for solar cells using localized surface plasmons," J. Appl. Phys. **105**(11), 114310 (2009).
19. D. Derkacs, S. H. Lim, P. Matheu, W. Mar, and E. T. Yu, "Improved performance of amorphous silicon solar cells via scattering from surface plasmon polaritons in nearby metallic nanoparticles," Appl. Phys. Lett. **89**(9), 093103 (2006).
20. P. Matheu, S. H. Lim, D. Derkacs, C. McPheeters, and E. T. Yu, "Metal and dielectric nanoparticle scattering for improved optical absorption in photovoltaic devices," Appl. Phys. Lett. **93**(11), 113108 (2008).
21. K. Nakayama, K. Tanabe, and H. A. Atwater, "Plasmonic nanoparticle enhanced light absorption in GaAs solar cells," Appl. Phys. Lett. **93**(12), 121904 (2008).
22. I. M. Pryce, D. D. Koleske, A. J. Fischer, and H. A. Atwater, "Plasmonic nanoparticle enhanced photocurrent in GaN/InGaN/GaN quantum well solar cells," Appl. Phys. Lett. **96**(15), 153501 (2010).
23. V. E. Ferry, L. A. Sweatlock, D. Pacifici, and H. A. Atwater, "Plasmonic nanostructure design for efficient light coupling into solar cells," Nano Lett. **8**(12), 4391–4397 (2008).
24. P. N. Saeta, V. E. Ferry, D. Pacifici, J. N. Munday, and H. A. Atwater, "How much can guided modes enhance absorption in thin solar cells?" Opt. Express **17**(23), 20975–20990 (2009).
25. J. Zhu, C.-M. Hsu, Z. Yu, S. Fan, and Y. Cui, "Nanodome solar cells with efficient light management and self-cleaning," Nano Lett. **10**(6), 1979–1984 (2010).
26. A. Lin, and J. Phillips, "Optimization of random diffraction gratings in thin-film solar cells using genetic algorithms," Sol. Energy Mater. Sol. Cells **92**(12), 1689–1696 (2008).
27. O. Isabella, A. Campa, M. C. R. Heijna, W. Soppa, R. van Ervan, R. H. Franken, H. Borg, and M. Zeman, "Diffraction gratings for light trapping in thin-film silicon solar cells," Conference Record of the 23rd European Photovoltaic Solar Energy Conference, 2320–2324 (2008).
28. C. Eisele, C. E. Nebel, and M. Stutzmann, "Periodic light coupler gratings in amorphous thin film solar cells," J. Appl. Phys. **89**(12), 7722–7726 (2001).
29. C. Haase, and H. Stiebig, "Thin-film silicon solar cells with efficient periodic light trapping texture," Appl. Phys. Lett. **91**(6), 061116 (2007).
30. K. Sato, Y. Gotoh, Y. Wakayama, Y. Hayasahi, K. Adachi, and H. Nishimura, "Highly textured SnO2:F TCO films for a-Si solar cells," Rep. Res. Lab. Asahi Glass Co. Ltd. **42**, 129–137 (1992).
31. V. E. Ferry, M. A. Verschuuren, H. B. T. Li, R. E. I. Schropp, H. A. Atwater, and A. Polman, "Improved red-response in thin film a-Si:H solar cells with soft-imprinted plasmonic back reflectors," Appl. Phys. Lett. **95**(18), 183503 (2009).
32. C. Stuart, and Y. Chen, "Roll in and roll out: a path to high-throughput nanoimprint lithography," ACS Nano **3**(8), 2062–2064 (2009).
33. M. Verschuuren and H. van Sprang, "3D photonic structures by sol-gel imprint lithography," Mater. Res. Soc. Sym. Proc. **1002**, N03–N05 (2007).
34. T. W. Odom, J. C. Love, D. B. Wolfe, K. E. Paul, and G. M. Whitesides, "Improved pattern transfer in soft lithography using composite stamps," Langmuir **18**(13), 5314–5320 (2002).
35. A. D. Rakic, A. B. Djurisic, J. M. Elazar, and M. L. Majewski, "Optical properties of metallic films for vertical-cavity optoelectronic devices," Appl. Opt. **37**(22), 5271–5283 (1998).
36. H. B. T. Li, C. H. M. van der Werf, J. K. Rath, and R. E. I. Schropp, "Hot wire CVD deposition of nanocrystalline silicon solar cells on rough substrates," Thin Solid Films **517**(12), 3476–3480 (2009).

1. Introduction

Thin-film solar cells offer the benefits of reduced materials and fabrication costs as well as the advantages of light-weight, flexible devices [1]. For these geometries to exhibit efficient current generation, light trapping schemes are essential to capture the red and near-infrared portion of the solar spectrum [2,3]. Here we demonstrate a hydrogenated amorphous Si (a-Si:H) solar cell with plasmonic light trapping structures built into the metallic back contact. The nanopatterns allow ultrathin a-Si:H cells (160 nm) with short circuit current densities exceeding that of similar cells with randomly-textured back contacts due to near-field coupling to guided modes supported by the multi–layer solar cell structure. The nanopatterns are fabricated via an inexpensive and scalable imprinting technique that could be adopted into standard solar cell production. We use a-Si:H as a test platform for photonic nanopattern design, but our approach is broadly applicable to other thin-film solar cell material systems.

Thin film solar cells made from a-Si:H are attractive candidates for large-scale photovoltaic applications because Si is highly abundant and can be deposited on flexible substrates using processes that are compatible with roll-to-roll processing [4]. Since minority

#128370 - $15.00 USD Received 12 May 2010; revised 7 Jun 2010; accepted 8 Jun 2010; published 24 Jun 2010

carrier diffusion lengths are very short in a-Si:H, the cells are often made with a p-i-n or n-i-p structure where the intrinsic absorbing layer is hundreds of nanometers thick and carrier transport is dominated by drift. Ultrathin film cells, where the thickness of the absorber layer is significantly reduced, offer further cost and performance advantages. An ultrathin film absorbing layer exhibits decreased bulk recombination, which can lead to a higher open circuit voltage (V_{oc}), since V_{oc} increases with decreasing dark current I_{dark} as $V_{oc} = (kT/q)\ln(I_{photo}/I_{dark} + 1)$ [5]. A final important benefit of this ultrathin film design for a-Si:H is the reduction of the well-known Staebler-Wronski degradation effect [6] that has limited the long-term performance of a-Si:H photovoltaics so far. Ultrathin n-i-p devices, with thicknesses such as we discuss here, possess high internal electric fields, which are known to exhibit no or only minimal light-induced degradation [4,7,8].

However, the use of thin absorbing layers reduces the short-circuit current density (J_{sc}) due to the decreased optical path length in the semiconductor. Strategies for increasing J_{sc} generally involve the incorporation of surface texturing to scatter incident light into off-normal angles. In thick, wafer-based photovoltaic cells, such surface texturing can lead to a maximum intensity enhancement of $4n^2$ at wavelengths near the band edge, where n is the index of refraction of the semiconductor [9]. For thin and ultrathin film cells where the total device thickness may be less than a wavelength, light trapping is frequently accomplished through the use of randomly roughened layers, either on the front or rear of the cell [10–12].

Recently, it has been proposed that the incorporation of plasmonic metal nanostructures in thin film solar cells could lead to strong light trapping because strong light-matter interaction in plasmonic nanostructures enables large scattering cross sections [13,14]. Many of these plasmonic photovoltaic designs incorporate metal nanoparticles on the front surface of the cell. This can lead to preferential scattering of the incident light into the semiconductor over an increased angular range, thereby enhancing the optical path length [15–22]. While strong enhancements of photocurrent have been reported in such solar cells for near-bandedge light, these are often offset by a reduced photocurrent in the blue part of the solar spectrum due to destructive Fano interference [18,21]. An alternative strategy is to build the scattering nanostructures directly into the back contact of the device. In this geometry, the incident blue light is directly absorbed and does not interact with the back contact scatterers, while the red light that is poorly absorbed in a single pass through the cell is strongly scattered [Fig. 1(a)] [23–25]. In our design, these back scatterers are designed to couple incident light into guided modes supported by the cell with high intensity in the absorbing semiconductor layer, dramatically reducing the thickness requirements by redirecting the absorption path into the plane of the solar cell. As opposed to cells with purely grating-based reflectors [26–29] or nanostructure designs to couple specifically to surface plasmon polariton modes [23], the design presented here takes advantage of the high scattering cross sections of plasmonic nanostructures to couple to waveguide modes.

To date most theoretical and experimental studies of plasmonic light trapping structures reference the enhanced absorption and photocurrent relative to an identical device without nanostructures (i.e., a planar back surface). While this reference is useful for understanding the role of the scatterers, most realistic solar cells already employ some form of light trapping structures to enhance absorption. For a-Si:H, much work has been devoted to the design of randomly textured layers for increased absorption [2–4,10–12], and we compare our plasmonic nanostructure designs to a commercial standard with known roughness and topography, Asahi U-type glass [30]. Provided that the plasmonic nanostructures are well-designed over the scale of a wavelength, we show here that the absorption enhancements can exceed those from random surface topography.

#128370 - $15.00 USD Received 12 May 2010; revised 7 Jun 2010; accepted 8 Jun 2010; published 24 Jun 2010

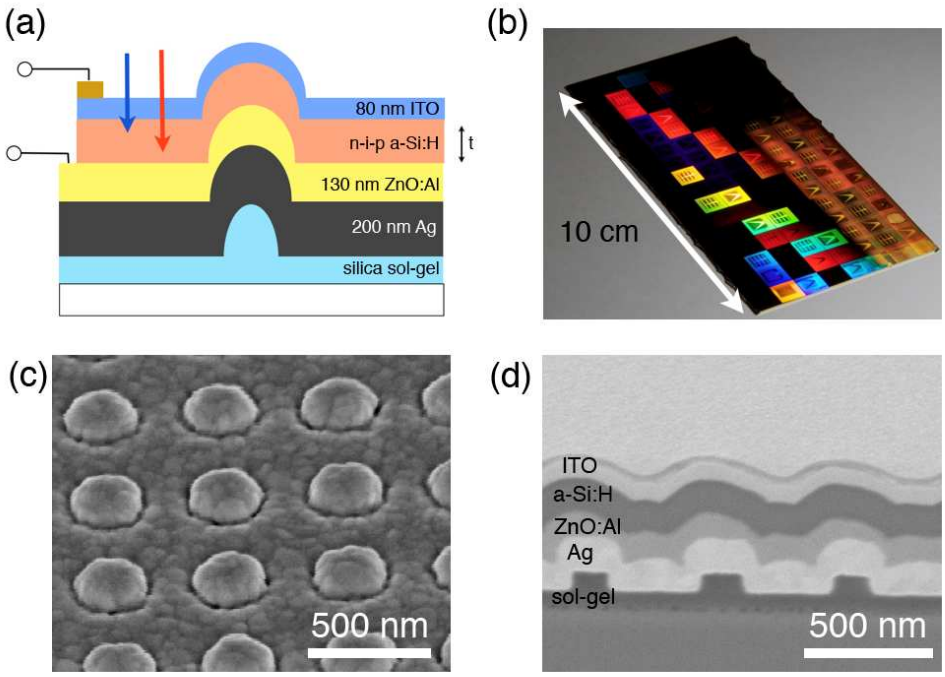

Fig. 1. Plasmonic light trapping solar cell design. (a) Schematic cross section of the patterned solar cell. Patterns are made on the rear glass substrate, and there is conformal deposition of all layers over the patterns through the top ITO contact. Incident blue and red arrows indicate that blue light is absorbed before reaching the back contact while red light interacts more with the back patterns. (b) Photograph of finished imprinted patterned solar cell substrate. Each colored square is a separate device, with different particle diameter and pitch. (c) SEM of Ag overcoated patterns showing 290 nm diameter particles with 500 nm pitch. (d) SEM image of a cross section of a fabricated cell, cut using focused ion beam milling. Note that the ultrathin a-Si:H layer constitutes only a small part of the cell.

2. Methods

A significant challenge to the incorporation of plasmonic nanostructures in photovoltaics is fabrication: the feature sizes are typically tens to hundreds of nanometers, while photovoltaic cell dimensions may be in the m^2 range. Techniques for large area metal nanostructure formation include island annealing, which produces irregular shapes and spacings [15,16], colloidal particles [19,20], which control the shape but not the spacing, and deposition through alumina templates, which can provide some control over the patterns [21,22]. Smaller test devices may use electron-beam lithography or focused ion beam patterning, which allow for complete control but are too expensive for use in practical devices. In this work, we have fabricated cm^2-scale a-Si:H solar cells using soft nanoimprint lithography [31] to incorporate plasmonic nanostructures in the Ag/ZnO:Al back contact of the cell [Fig. 1(b)]. This technique offers the capability to form large-area nanopatterns with precise control over both the dimensions and the spacing of the plasmonic scattering structures, and is amenable to roll-to-roll processing [32]. In our case, the patterns are printed into a sol-gel silica layer using substrate conformal imprint lithography (SCIL) [33], which is then overcoated with Ag and

#128370 - $15.00 USD Received 12 May 2010; revised 7 Jun 2010; accepted 8 Jun 2010; published 24 Jun 2010

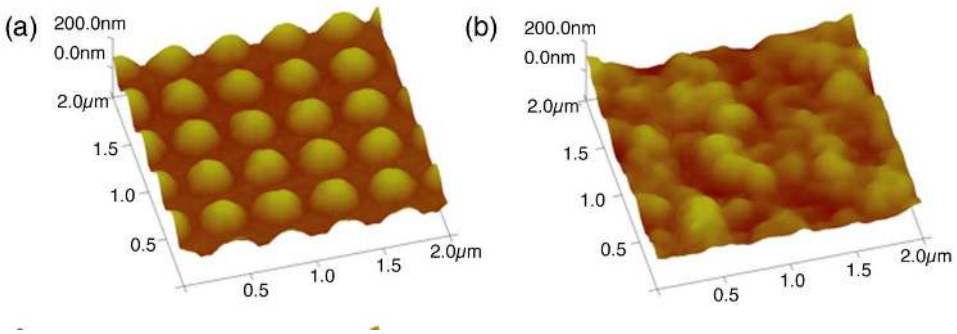

Fig. 2. Surface topography of nanopatterned and randomly textured solar cells. Tapping-mode AFM images of the top ITO contacts for two of the cells compared in this study. The underlying Ag/ZnO:Al nanostructure is transferred through each layer conformally, so that both the front and back contacts are structured. (a) Patterned cell with 500 nm pitch, (b) Cell on randomly textured Asahi U-type glass substrate.

ZnO:Al to form the back contact [Fig. 1(c)]. A single substrate containing solar cells with nanopatterns of varying diameter and pitch as well as reference cells with flat back contacts is used to avoid variations between different deposition runs when comparing cell performance, shown in Fig. 1(b).

The master substrate of nanopatterns was made using electron beam lithography on a Si wafer. A bilayer stamp was molded from the master, consisting of a thin high-modulus polydimethylsiloxane (PDMS) layer holding the nanopatterns and a low-modulus PDMS layer to bond the rubber to a 200 μm thick glass support for in-plane stiffness [34]. The stamp was used to emboss a 100 nm thick layer of silica sol-gel on AF45 glass substrates using SCIL. The sol-gel layer solidified at room temperature by forming a silica network, while reaction products diffuse into the rubber stamp. After stamp release the sol-gel was post cured at 200 °C. The patterned area was 10 cm by 4 cm, with patterned and flat reference cells tiled in 6 mm x 6 mm sections. The sol-gel patterns together with the Asahi U-type glass were overcoated with Ag and ZnO:Al via sputtering, and 13.56 MHz plasma enhanced chemical vapor deposition was used to deposit the n-i-p a-Si:H layers. An array of 4×4 mm^2 squares of ITO was sputtered through a contact mask, and finger contacts were evaporated over the ITO using a second contact mask. The final cell area of each device was 0.13 cm^2. Device characterization was performed using a solar simulator under one sun illumination (AM1.5, 100 mW/cm^2) and EQE measurements were performed using monochromatic light from a Xenon lamp with one sun light bias applied. Angle-resolved EQE measurements were performed using a supercontinuum laser source in combination with a monochromator with a passband of ~3 nm and a sample stage providing eucentric rotation about the point of illumination. The illumination was focused to a spot diameter of approximately 500 μm at low numerical aperture. Finite-difference time domain simulations (FDTD) were performed using commercially available software. The layer thicknesses were taken from cell cross sections [such as Fig. 1(d)]. The optical constants of the ITO and ZnO:Al were taken as 2.08 + 0.004i and 1.93 + 0.004i, respectively, with slight dispersion measured using ellipsometry. The optical data for a-Si:H was taken from measured values. Ag was modeled using a Lorentz-Drude model fit to Palik data [35]. The simulation geometry for the randomly textured cells was taken from measured AFM data, and used to construct the surface.

Multiple copies of each cell design and reference are distributed over the substrate to reduce the possible effects of wafer-scale spatial inhomogeneity, and several cells of each pattern were measured. Two different intrinsic layer thicknesses, corresponding to total a-Si:H thicknesses (including the n- and p-doped layers) of 340 nm and 160 nm were deposited on

#128370 - $15.00 USD Received 12 May 2010; revised 7 Jun 2010; accepted 8 Jun 2010; published 24 Jun 2010

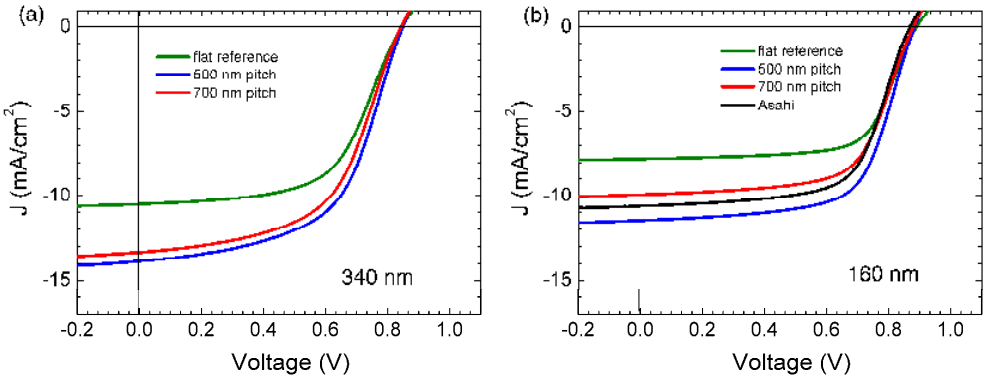

Fig. 3. Electrical measurements on plasmonic solar cells. Data are shown for a-Si:H with two different intrinsic layer thicknesses. (a) a-Si:H thickness 340 nm and (b) a-Si:H thickness 160 nm. Curves are shown for square grid patterns of 250 nm diameter plasmonic scatterers at pitches of 500 nm and 700 nm, the flat reference cell, and (in (b)) the randomly textured Asahi cell.

two substrates with identically prepared back contact patterns. Figure 1(d) shows a cross section scanning electron microscopy (SEM) image of a fully fabricated nanopatterned cell having ana-Si:H thickness of 160 nm. The individual layers are clearly resolved. The ultrathin a-Si:H layer is conformal to the nanopatterned contacts, with no cracks or voids observed in the layer that could adversely influence the performance [36]. In addition to the substrates patterned by imprint lithography, a randomly textured substrate of Asahi U-type glass was used to simultaneously fabricate a 160 nm thick a-Si:H cell under the same deposition conditions as the nanopatterned substrate.

Since each successive layer is conformally deposited, the underlying back contact structure for both the patterned and the randomly textured devices is transferred to the top interface of the cell. Figure 2 shows tapping mode atomic-force microscopy (AFM) scans on the indium tin oxide (ITO) top contact for both the imprint-patterned cell (a) and the randomly textured Asahi sample (b). The imprinted substrate AFM scan reveals the underlying 175 nm diameter nanopatterns that are imprinted into the sol-gel glass layer, and transferred to the back contact of the cell at a pitch of 500 nm. In contrast, the randomly textured Asahi glass shows an uncorrelated distribution of height variations.

3. Results

Figure 3 shows current density/voltage (J-V) measurements taken under 100 mW cm^{-2} AM1.5 illumination for the 340 nm (a) and 160 nm (b) thick cells, all for cells with a plasmonic scatterer diameter of 250 nm. In Fig. 3(a), data for 500 nm and 700 nm pitch are shown together with the flat reference. In Fig. 3(b), data for the randomly textured Asahi glass cells are also shown. For the 340 nm cells, the V_{oc} is in the 840–850 mV range for all devices measured, indicating that there is no significant difference in semiconductor and contact quality across the substrate. Data taken for several Ag particle diameters (200 nm, 225 nm, 250 nm, 290 nm) all show similar J_{sc}, V_{oc}, and fill factor characteristics, with a slight increase in performance for larger diameter scatterers. However, a higher J_{sc} is found for cells with a 500 nm pitch than for cells with a 700 nm plasmonic scatterer pitch. For the 500 nm pitch samples, J_{sc} improves by 27% compared to the flat cell. The highest efficiency recorded among cells with the 340 nm thick a-Si:H layer (η = 6.6%) was found for a plasmonic scatterer pitch of 500 nm and a diameter of 250 nm.

For the thinner cells [Fig. 3(b)], V_{oc} is increased in comparison to the thicker cells, to around 880-890 mV. We attribute this improvement to the decreased bulk recombination in thin layers demonstrating, as mentioned previously, an additional important advantage of the use of thin active layers aside from the reduced costs [5]. At the same time, the fill factors

#128370 - $15.00 USD Received 12 May 2010; revised 7 Jun 2010; accepted 8 Jun 2010; published 24 Jun 2010

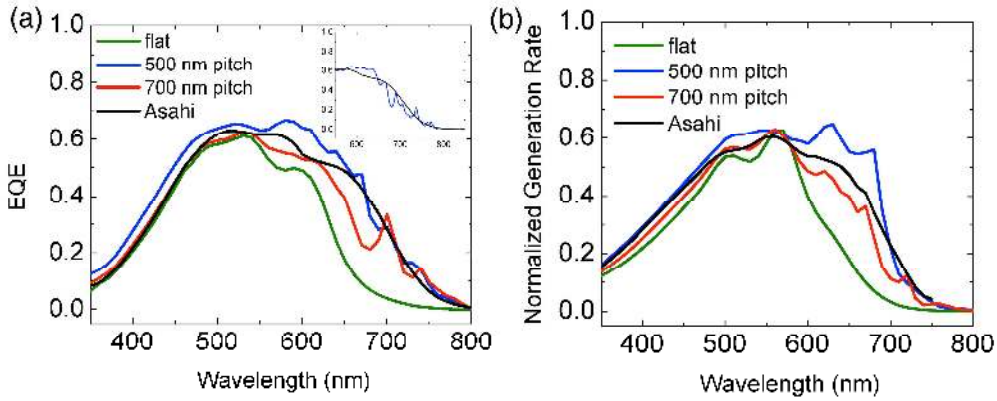

Fig. 4. External quantum efficiency spectra of nanopatterned and randomly textured cells from measurement and simulation. EQE spectra are shown in (a) for cells of thickness 160 nm, under one sun illumination at 0V bias. The primary enhancement in photocurrent over the flat reference cell occurs from 550 - 800 nm. The 500 nm pitch cell shows higher EQE than the randomly textured Asahi cell. The inset of (a) shows EQE measurements of these two cells at higher spectral resolution. Electromagnetic simulations of the generation rate spectra are shown in (b) for the same set of devices.

have increased to 0.64. The 500 nm pitch, 250 nm diameter samples now show an increase in J_{sc} of 46% over the 160 nm thick flat cell. The best cell measured again had 250 nm diameter plasmonic scatterers and 500 nm pitch. This cell has an efficiency of 6.6%, which is similar to the maximum efficiency found for the thick cell. While J_{sc} is lower in the thin cells, the increased V_{oc} and fill factor cause the overall efficiency to remain the same between the two thicknesses. This demonstrates conclusively that plasmonic back reflectors can be used to maintain efficiency while scaling to thinner solar cells. The J_{sc} of the 500 nm patterned cell is improved by 50% compared to the flat reference cell.

Remarkably, Fig. 3(b) also shows that J_{sc} for the patterned cell with 500 nm pitch is significantly larger than for the randomly textured cell with Asahi-U type of texture. Because the nanopatterned cells and the randomly textured Asahi sample both have comparable fill factor and V_{oc}, we can exclude a difference in semiconductor quality as an explanation for the improved J_{sc}. We conclude that light trapping in the 500 nm pitch patterned cell is more efficient than in the randomly textured sample.

4. Discussion

To further study the nature of the photocurrent enhancement, we measured external quantum efficiency (EQE) spectra, defined as the number of collected charge carriers per incident photon, using a Xenon lamp under light bias corresponding to approximately one sun illumination and 0 V bias. Figure 4(a) shows the EQE spectra for the same thin cells described in Fig. 3(b). We note a slight increase in photocurrent on the blue side of the band for the 500 nm pitch cell, from 350 nm – 550 nm, which we attribute to improved anti-reflective properties of the corrugated top surface of the cell. The primary photocurrent enhancement occurs in the 550 nm–800 nm spectral range. While the EQE of both the 500 nm and the 700 nm pitch cells exceeds that of the flat reference cell, there is a pronounced difference between the curves in the wavelength range from 550 nm to 700 nm. The cell on the randomly textured Asahi substrate has a very smooth EQE response, while the patterned devices exhibit peaked features in the EQE curve, of which the peak wavelengths are reproducible for each pitch. The inset of Fig. 4(a) shows EQE spectra of these two cells recorded with higher spectral resolution using a supercontinuum laser source filtered by a grating spectrometer. The complex structure of the 500 nm pitch sample remains clearly visible compared to the smooth EQE spectrum of the randomly textured Asahi sample. Notably, the EQE of the 500 nm pitch cell exceeds that of the randomly textured Asahi sample in the 550–650 nm spectral range

#128370 - $15.00 USD Received 12 May 2010; revised 7 Jun 2010; accepted 8 Jun 2010; published 24 Jun 2010

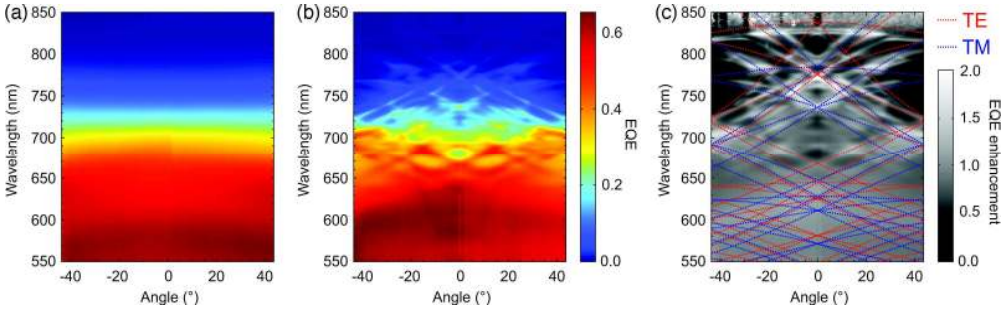

Fig. 5. Angle-resolved photocurrent spectroscopy. Measured EQE versus incident wavelength and incident angle for (a) the randomly textured Asahi cell and (b) the 500 nm pitch nanopatterned cell with 160 nm a-Si:H thickness. The Asahi cell shows a rather isotropic angular response, while the nanopatterned sample shows clear evidence of grating coupling to guided modes. The EQE enhancement for the nanopatterned sample, the ratio of (b) to (a), is shown in **c**; the calculated folded-zone dispersion diagram of the lowest-order TE and TM modes is superimposed.

where there is significant power in the solar spectrum. From 650 nm to 800 nm the features in the spectra of the nanopatterned cell sharpen and alternately exceed and fall below the curve for the randomly textured Asahi cell.

We use full-field finite difference electromagnetic simulations to study the integrated carrier collection rate from the nanostructured cell, with the cell layer thicknesses and optical constants taken from experimental values. Figure 4(b) shows the calculated carrier generation rate in the a-Si:H, modeled as $G_{opt} = \varepsilon''|E|^2/2\hbar$, normalized by the incident photon flux across the 350–800 nm. Our model assumes a geometry to describe the two patterned cells, where the nanostructures are taken to be hemispheres and the unit cell is chosen with either 500 or 700 nm pitch and periodic boundaries. The surface structure for the randomly textured Asahi cell was modeled using the AFM data shown in Fig. 2. The optical model accurately reproduces the spectral shape of the curves, including the enhanced absorption of the 500 nm pitch cell relative to the randomly textured cell and the reduced absorption for the 700 nm pitch cell. The enhancement and many of the peaked features are reproduced well in the simulation, and deviations may be due to minor variations in layer thickness, pitch, optical constants, and differences between the real and assumed nanostructure geometry. The overall spectral correspondence between the electromagnetic simulation and the EQE measurements strongly suggests that the EQE enhancement is due to increased absorption from light trapping.

To further investigate the nature of the light trapping mechanism for the nanopatterned and randomly textured Asahi glass samples we measured EQE spectra as a function of incident angle for the thinner cells. Figure 5 shows intensity maps of these angle-resolved EQE spectra, for angle of incidence between −45° and + 45° from the substrate normal and for a range of illumination wavelengths from 550 nm to 850 nm, for the randomly textured Asahi cell [Fig. 5(a)] and the 500 nm pitch cell [Fig. 5(b)]. The EQE curves at normal incidence were found to agree well with the measurements shown in Fig. 4. Some variation with angle of incidence is expected for all cells due to the angular response of the anti-reflection coating present on the cells. However, while it is evident that the randomly textured Asahi cell has a relatively isotropic spectral response to angle of incidence, the 500 nm pitch cell exhibits more complex behavior. The enhanced EQE for the patterned cell in the 550–650 nm range [inset in Fig. 4(a)] is observed, and can be seen to extend to at least ± 20 degrees. From 650 to 800 nm the spectral photocurrent features become sharper, and show a stronger angular dependence. The dispersive features measured in Fig. 5(b) are clear evidence of coupling between light scattered by the grating and the guided modes supported by the high-index a-Si:H layer of the solar cell.

We calculated the dispersion curves for the guided modes present in a representative planar device with 500 nm periodicity. The calculations were performed using the

#128370 - $15.00 USD Received 12 May 2010; revised 7 Jun 2010; accepted 8 Jun 2010; published 24 Jun 2010

experimentally determined layer thicknesses and optical constants. In Fig. 5(c), branches corresponding to the TE and TM modes with the highest modal overlap with the a-Si:H are shown, folded back to the angular range of interest by taking diffraction by the two-dimensional periodic structure into account. The curves are superimposed over an intensity map of the relative enhancement of the EQE of the patterned cell compared to the randomly textured Asahi cell. Clearly, the pattern of dispersive bands observed in the EQE measurements agrees well with the calculated mode dispersion. In particular, the bands of enhanced absorption in the 700–850 nm range are well explained by the model, including the crossings at 740 nm and 770 nm. Deviations between measurement and calculation are attributed to small differences in optical constants and the fact that the calculation does not include surface corrugation and associated mode coupling. Additional spectral features observed in the EQE spectra could possibly be associated with absorption due to local field enhancements in the nanostructures. The measurement clearly shows that for these wavelengths, coupling to modes guided by the a-Si:H layer is responsible for increased absorption in the cell. Calculations show a high density of modes in the spectral range 550–650 nm where the EQE of the patterned cell exceeds that of the randomly textured Asahi substrate. The fact that in this region no sharp features are observed in the measurements is due to the large number of modes present, which are strongly broadened because of large absorption of a-Si:H in this spectral region. Although similar modes may be observed for patterned dielectric particles, the scattering cross section of the metal nanostructures increases coupling to the guided modes, further enhancing the photocurrent.

5. Conclusion

In summary, we have demonstrated ultrathin (160 nm) a-Si:H solar cells with efficient light trapping by a nano-engineered plasmonic back reflector. Light is scattered strongly from the nanopatterned metal back contact into guided modes of the cell, enhancing the photocurrent for a given cell thickness by enhancing the coupling to the modes. Similarly, the same photocurrent can be achieved at a reduced cell thickness, with a concomitant increase in open circuit voltage (and potential for increased long-term stability). We demonstrate that nano-engineered cells show light trapping that is enhanced beyond that of a randomly textured cell. This new design is not strictly relevant to a-Si:H based devices, but may be broadly applicable to other common thin-film solar cell materials systems such as polycrystalline Si, CdTe, and $CuIn_xGa_{1-x}Se_2$. This result can directly impact the attainment of economically competitive and scalable renewable energy from thin-film solar cells.

Acknowledgements

C. H. M. van der Werf is acknowledged for solar cell depositions, L. A. Sweatlock for insights in FDTD simulations, and R. de Waele and I. M. Pryce for discussions. The Caltech portion of this work was supported by the Department of Energy under contract number DE-FG02-07ER46405 (modeling) and SETP GO-18006 (cell fabrication). Work at AMOLF is part of the research program of FOM which is financially supported by NWO. The work at Utrecht University was fully supported internally. This work is part of the Smart-Mix program Memphis and the Global Climate and Energy Project (GCEP).

#128370 - $15.00 USD Received 12 May 2010; revised 7 Jun 2010; accepted 8 Jun 2010; published 24 Jun 2010